Far Field of Bragg Reflection Waveguides: Characteristics and Closed-Form Approximation

Nima Zareian, Payam Abolghasem, *Member, IEEE*, and Amr S. Helmy, *Senior Member, IEEE, Member, OSA*

***Abstract*—A comprehensive study of the far-field diffraction pattern of Bragg reflection waveguides is presented. Using a Gaussian approximation of the near-field profile, an analytical formula for the far-field pattern of the fundamental Bragg mode is obtained. The proposed closed-form representation offers a powerful technique for examining the far-field characteristics, which provides insight into the design optimization of Bragg reflection waveguides.**

***Index Terms*—Bragg reflection waveguides (BRWs), diffraction theory, far field, transverse Bragg reflector.**

I. Introduction

BRAGG REFLECTION waveguides (BRWs) were initially proposed in 1976 [1], [2]. However, these structures were not fully exploited in photonic applications except years later. This is likely due to the demanding tolerances required for epitaxy and fabrication to realize devices from these structures and the state of these technologies at the time. Recently BRWs have found applications in numerous novel photonic devices. These include mechanically tunable air-core filters [3], polarization splitters [4], hollow-core sensors [5], and nonlinear frequency converters [6], [7], only to name a few.

Owing to their dispersive properties, BRWs are an attractive means to achieve phase matching of optical nonlinearities in a monolithic platform, where optoelectronic devices are realized [8]. Their implementation in nonlinear optical applications has led to record conversion efficiencies, utilizing second order nonlinear effects in semiconductors recently [7]. Prior to these recent demonstrations, various techniques have been devised to achieve phase matching in semiconductors [9]–[11]. However BRWs offer an optimal platform for active and passive integration of laser sources on the same chip, where phase matching is achieved. This could enable an array of otherwise unavailable monolithic devices that utilize parametric nonlinear optical effects.

In integrated devices incorporating BRWs, analysis of the radiation pattern of the guided modes is essential for obtaining a thorough understanding of the strengths and limitations of these structures in interfacing with other components in any optical system. If these devices are to be used in an integrated monolithic setting, a key parameter in analyzing the optical radiation is the far field (FF). To the best of our knowledge, no previous work has been carried out on systematic analysis of the far-field patterns of modes in BRWs. The performance and figures of merit associated with applications utilizing BRWs such as frequency conversion and edge-emitting BRW-based lasers depend on a suitable far-field profile for these structures, which is the motivation of this work.

Single-sided BRW lasers have been implemented previously [12]. Lasers based on dual-sided BRWs have also been proposed theoretically [13] and were demonstrated recently [14]. In earlier theoretical studies [13], the dual-lobed nature of the far field of the fundamental mode of some BRW configurations has been identified as an impediment for efficient out-coupling of light. This is because of its incompatibility with other guided-wave structures and optical fibers, where Gaussian-like profiles of fundamental total internal reflection (TIR) modes are more common. This work suggested less practical solutions such as phase masks to alter the far field [13], inspired by work from the field of diode laser arrays [15]. Although the FF of BRWs has seldom been investigated, there has been a significant effort in the related area of combining and manipulating the FF of diode laser arrays [15]–[17]. Different methods have been proposed for achieving single-lobed operation of such arrays. One such approach is via the application of phase masks, either integrated [15], or implemented using discrete spatial elements [18], [19]. However, these methods are not suitable for the case of monolithic single-mode BRWs, as they need to be implemented on the cleaved facet of the device.

This work systematicaly investigates the FF properties of the lowest order even Bragg mode in BRWs. This mode is of particular interest as it has been widely employed in many applications [7]. The stark difference in behavior between the far field of this fundamental mode and that of a fundamental mode of a TIR waveguide will also be examined. In addition, this work will develop an approximate formulation to describe the FF of the lowest order even Bragg mode in BRWs using a closed-form analytical formulation and define its domain of validity. Our analysis is based on the introduction of an approximation, that exploits the Gaussian expansion of an optical mode profile, which in turn leads to an analytical formulation for the FF of the fundamental Bragg mode. This analytic formulation for the far-field pattern provides insight into the design and optimization process of this type of waveguides. Using the approximation, novel insight into the properties of the FF is demonstrated and discussed.

Manuscript received June 03, 2010; revised October 15, 2010, December 01, 2010; accepted December 19, 2010. Date of publication December 30, 2010; date of current version February 28, 2011. This paper was supported by the Natural Sciences and Engineering Research Council of Canada (NSERC).

The authors are with the Edward S. Rogers Sr. Department of Electrical and Computer Engineering and the Institute of Optical Sciences, University of Toronto, Toronto, ON M5S 3G4, Canada (e-mail: a.helmy@utoronto.ca).

Color versions of one or more of the figures in this paper are available online at http://ieeexplore.ieee.org.

Digital Object Identifier 10.1109/JLT.2010.2102741

The organization of this paper is as follows. Section II provides a brief review of BRWs with analysis of their far-field profile and diffraction pattern. In Section III, a Gaussian approximation of the field-profile and the associated far-field pattern are discussed. Simulation results and design considerations with an outline for optimization of far-field pattern to be compatible with TIR-based waveguides and optical fibers are presented in Section IV. Conclusions are then given in Section V.

II. Bragg Reflection Waveguides

In contrast to conventional waveguides, where waveguiding relies on total internal reflection, BRWs utilize the stopband of transverse Bragg reflectors (TBRs) to provide Bragg reflection, and hence confinement of the guided waves. Detailed analysis of the modal properties of BRWs with quarter-wave TBRs was previously discussed in [20]. In this section, we briefly review the effective modal properties of BRWs, which are used for the analysis of diffraction characteristics and the calculations of the far-field profile.

The schematic of a slab BRW along with the index profile of the structure is illustrated in Fig. 1. The refractive indexes of the bi-layers of the TBRs are taken as n_1 and n_2 with associated thicknesses of t_1 and t_2 and with periodicity of $\Lambda = t_1 + t_2$. The core has a refractive index of n_c and a thickness of t_c. For the propagating mode with effective mode index of n_{eff}, the transverse wavevector within the j-th layer takes on discrete values as

$$k_j = k_0\sqrt{n_j^2 - n_{\text{eff}}^2} \tag{1}$$

where $j \in \{1, 2, c\}$ and k_0 is the wavevector in free space. Assuming the TBRs are semi-infinite and using the Bloch-Floquet formalism, dispersion equations for the fundamental TE and TM propagating Bragg modes can be expressed as [20]

$$\frac{1}{k_c}\cot\left(\frac{k_c t_c}{2}\right) = \frac{-i}{k_1}\left(\frac{n_1}{n_c}\right)^{2f}\frac{\exp(iK\Lambda) - A + B}{\exp(iK\Lambda) - A - B} \tag{2}$$

where $f = 0$ for TE propagation and $f = 1$ for TM propagation. In (2), the coefficients A and B are the elements of the unit-cell translation matrix and are defined as [1], [2]

$$A = \exp(ik_1t_1)\left[\cos(k_2t_2) + \frac{i}{2}\left(\frac{n_2^{2f}k_1}{n_1^{2f}k_2} + \frac{n_1^{2f}k_2}{n_2^{2f}k_1}\right)\sin k_2t_2\right]$$

$$B = \exp(-ik_1t_1 + if\pi)\left[\frac{i}{2}\left(\frac{n_2^{2f}k_1}{n_1^{2f}k_2} - \frac{n_1^{2f}k_2}{n_2^{2f}k_1}\right)\sin k_2t_2\right]. \tag{3}$$

Also, K is defined as the Bloch wavenumber which is [2]

$$\cos K\Lambda = \text{Re}\{A\}. \tag{4}$$

Here, we focus on the fundamental even Bragg mode, which is of chief interest to our analysis. For the even mode to exist, the conditions $n_1 > n_2$ and $n_2^2k_1 > n_1^2k_2$ should be satisfied for TE and TM polarizations, respectively. For quarter-wave TBRs, the accumulated phase in the bi-layers should be $k_1t_1 = k_2t_2 = \pi/2$. Operating at the quarter-wave condition is attractive for several reasons. For example, at this operating point, the highest reflection coefficient from Bragg mirrors is tenable and leads to maximum exponential decay for the guided mode in the periodic claddings, which guarantees maximum confinement in the core. Additionally, for quarter-wave Bragg reflection waveguides (QtW-BRWs) there exist simple analytical expressions for calculating the modal dispersion properties. In [20], it is shown that the lowest order Bragg mode for either TE or TM polarization states can be expressed as

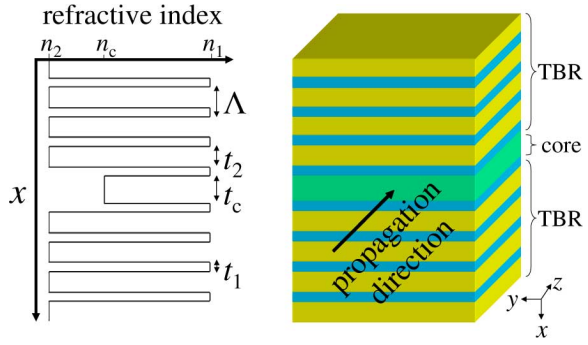

Fig. 1. Index profile of a generic Bragg waveguide.

$$n_{\text{eff}} = \sqrt{n_c^2 - \left(\frac{\pi}{k_0t_c}\right)^2}. \tag{5}$$

For a QtW-BRW, (4) can also be simplified as

$$\exp(iK\Lambda) = -\left(\frac{n_1}{n_2}\right)^{2f}\frac{k_2}{k_1}. \tag{6}$$

Field distribution in BRWs can be easily calculated using the transfer matrix method. Here, we use $\psi(x)$ to denote the transverse profile of the tangential electric/magnetic field for TE/TM polarizations. Using the Rayleigh-Sommerfeld diffraction integral with a minimum possible number of approximations leads to the diffraction formula [21], [22]

$$\Psi(\theta) = \cos(\theta)\int_{-\infty}^{+\infty}\psi(x)\exp[-ik_0x\sin(\theta)]dx \tag{7}$$

where θ is the observation angle from the direction of wave propagation and the term $\cos(\theta)$ provides a good approximation to the inclination factor [21]. In order to highlight the salient features of the FF as a function of the BRW attributes, three QtW-BRW design examples are considered. These examples are chosen to cover the range of waveguide dispersion behavior exhibited by this class of waveguides. In the examples the same structure is used, where only the core thickness is allowed to vary while the thicknesses of the bi-layers are designed to satisfy the quarter-wave condition. The structures are based on the GaAs/AlGaAs materials system. The Gehrsitz model [23] is used to calculate the refractive index of the layers for the calculations in this work. Table I lists the waveguide design parameters for the three BRWs.

We define a normalized effective index B, which is related to the normalized propagation constant used in the analysis of the total internal reflection waveguides, as

TABLE I
DESIGN PARAMETERS FOR EXAMPLES D_1 TO D_3. ALL THREE EXAMPLES OPERATE AT THE FREE SPACE WAVELENGTH OF $\lambda = 775$ nm

Design example	D_1	D_2	D_3
n_c	3.1714	3.1714	3.1714
n_1	3.5305	3.5305	3.5305
n_2	3.1771	3.1771	3.1771
t_c (nm)	140	700	3000
t_1 (nm)	61.1	117.6	124.4
t_2 (nm)	69.8	331.1	845.6
n_{eff}	1.5482	3.1227	3.1688

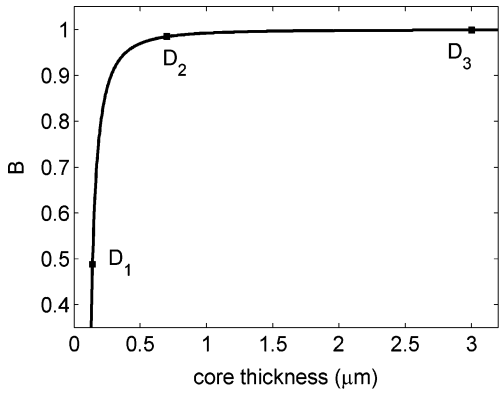

Fig. 2. Normalized effective index versus core thickness for various QtW-BRWs with core and cladding compositions identical to the waveguides in Table I at $\lambda = 775$ nm. The location of each design example is shown on the curve accordingly.

$$B = \frac{n_{\text{eff}}}{n_c} = \sqrt{1 - \left(\frac{\pi}{k_0 t_c n_c}\right)^2}. \tag{8}$$

The variation of B with t_c for waveguides of the given composition is shown in Fig. 2, and the location of each design example is highlighted on the curve.

The plots in Fig. 3 illustrate the field profiles of the fundamental TE modes for the design examples discussed above. The corresponding diffraction patterns are calculated using (7) and are plotted in Fig. 4 after normalization to their maximum. To further study the FF behavior in more detail, the far field of a range of QtW-BRWs is plotted as a function of core thickness and θ in Fig. 5. Here, the core and cladding compositions are identical to the examples given in Table I. In this figure, the core thickness ranges from 140 nm as in D_1 to 3000 nm similar to D_3. From the figure, three areas of operation can be defined: 1) an area in which FF is a non-confined single lobe for core thicknesses smaller than 250 nm; 2) a double-lobed FF operational area, which takes place for core thicknesses less than 1.4 μm; and 3) lastly an area of single lobe FF for larger core thicknesses, in which the full width at half maximum (FWHM) of the far field is inversely dependent on t_c as shown in Fig. 6.

The plot in Fig. 5 highlights two areas of high and low dispersion which lead to single lobed operation in the FF. The behavior within region (c) can be roughly explained as follows: As the core thickness increases, the field profile asymptotically approaches that of a conventional TIR waveguide with a single-lobed far field. At the same time, as the core increases in width,

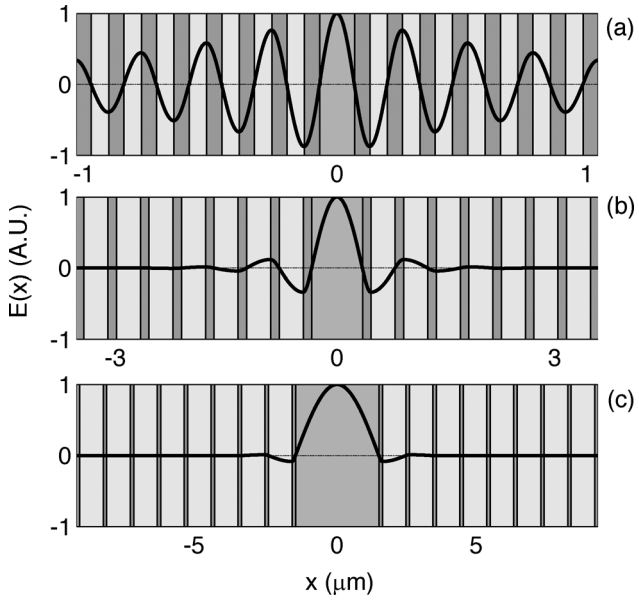

Fig. 3. Calculated near field of the fundamental TE Bragg mode for design examples (a) D_1, (b) D_2, and (c) D_3 with parameters listed in Table I.

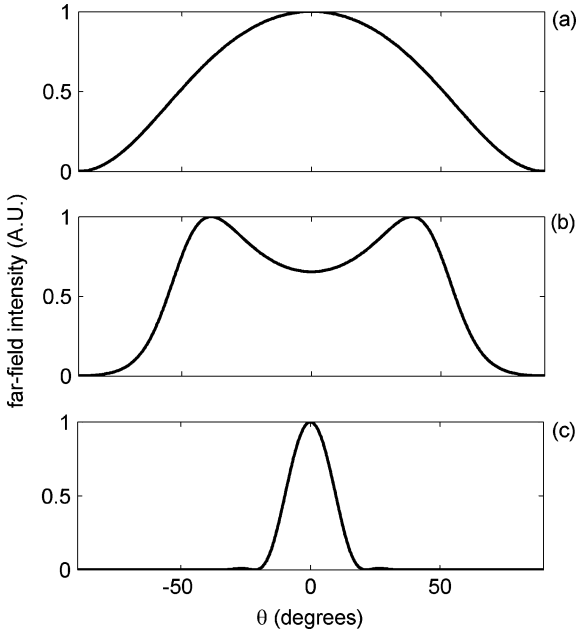

Fig. 4. Calculated far field of the fundamental TE Bragg mode for design examples (a) D_1, (b) D_2, and (c) D_3.

the FWHM of the far-field diffraction pattern is reduced, stemming from an enhanced confinement in the core. In contrast, the behavior within region (a) can be understood as one inspects the near field in this regime, which gets less localized in the center as the core layer thickness is reduced. This leads to a larger spread of the near field throughout the structure, which causes a reduction in the associated FF width.

There are two limitations which restrict the versatility of modes of operation similar to D_1 and hence make it less desirable in designing practical BRW structures. Far-field behaviors in area (a) usually take place when the BRW core is relatively thin and its refractive index is low compared to the cladding

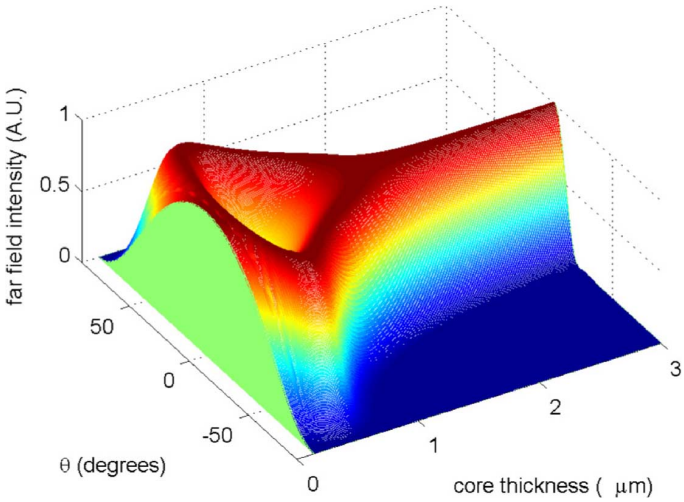

Fig. 5. Calculated far field of the fundamental TE Bragg mode at $\lambda = 775$ nm for a range of core thickness from 140 nm to 3000 nm.

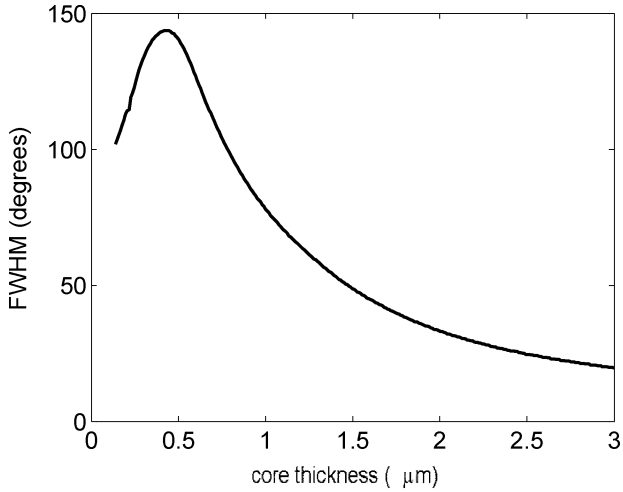

Fig. 6. Far-field FWHM of the fundamental TE Bragg mode at $\lambda = 775$ nm as a function of core thickness.

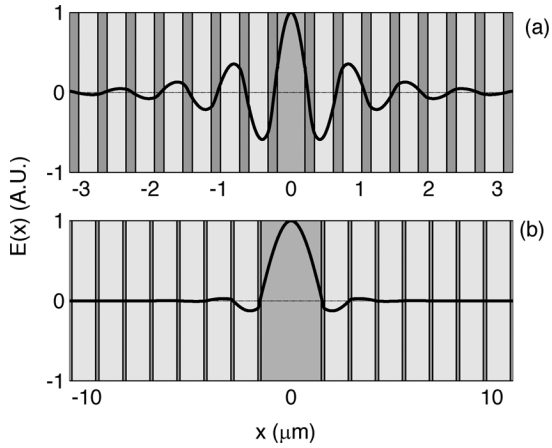

Fig. 7. Calculated near field of the fundamental TE Bragg mode for design examples (a) D4 and (c) D5 with parameters listed in Table II.

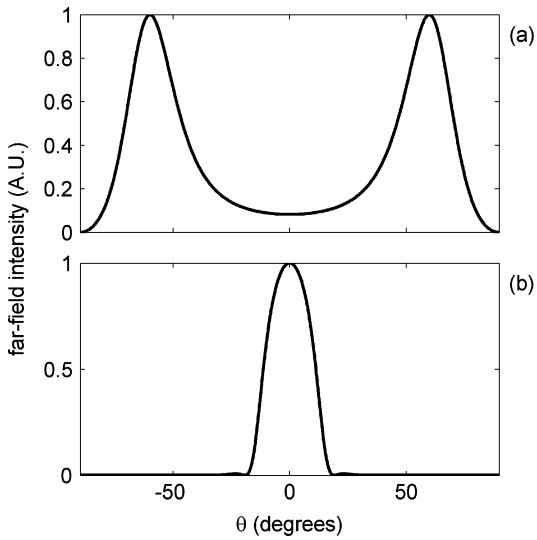

Fig. 8. Calculated far field of the fundamental TE Bragg mode for design examples (a) D_4 and (b) D_5.

layers. Due to the comparatively low effective modal index associated with such a waveguide mode, the reflectivity from the Bragg mirrors is very low. This renders the modal loss intolerable in TBRs with a finite number of Bragg reflectors, where the low confinement gives rise to a large leakage loss. Moreover, in these cases, despite being a single lobe, the FF divergence is significant in comparison to region (c). As described earlier, in order to enable efficient coupling between a BRW-based device and other optical components, the FF needs be single-lobed, with minimal divergence.

Operating at the QtW point does not only result in maximum confinement in the BRW core, but also it provides analytical formulae for the device parameters, which affords greater insight into the device design process. However, the BRW can be designed in many other fashions to avoid the extra restrictions posed by the QtW condition. The FF behavior examined in the case of QtW-BRWs above also manifests itself in generic BRWs. Table II introduces two more design examples, which have been chosen to highlight the range of FF properties exhibited by non-QtW-BRWs. The near field and far field of the examples are illustrated in Figs. 7 and 8 respectively. In case of general BRWs, there is a larger number of variables that can alter the FF behavior. This makes it less tangible to document the behavior in a plot similar to that given in Fig. 5. Nevertheless, the same trend as that described for QtW-BRWs can be found in the two examples D_4 and D_5.

Although the presented interpretation can partly elucidate the behavior of the given design examples, it can not provide a distinct boundary for different modes of FF operation. The far field

TABLE II
DESIGN PARAMETERS FOR THE NON-QWS EXAMPLES, D_4 AND D_5. BOTH EXAMPLES OPERATE AT $\lambda = 775$ nm

Design example	D_4	D_5
n_c	3.1714	3.1714
n_1	3.5305	3.5305
n_2	3.1771	3.1771
t_c (nm)	400	2000
t_1 (nm)	137.7	161.8
t_2 (nm)	274.8	118.4
n_{eff}	3.0754	3.1690

is dependent not only on the core thickness, but also the waveguide geometry and the operating point on the dispersion curve of a given design. As such, it is not possible to derive a simple relation for the core thickness to predict the FF properties just by inspecting different examples as done here.

In this work, we used numerical integration to calculate the far-field diffraction pattern and predict the FF properties. However, the advantage of having the insight of designing the device using analytical closed form expressions is not available when using such integration techniques. Consequently, the presented explanation does not provide insight in the design and optimization process of BRWs. A more intuitive understanding will significantly assist in the optimization of BRW structures for numerous applications. This is indeed possible if a prediction of the FF pattern of the fundamental mode of the BRWs can be obtained via an analytical approach. We shall demonstrate the availability of analytic approximation for the FF intensity of the fundamental Bragg mode in the next section based on a methodology similar to [16], [17].

III. Gaussian Approximation of the Field Profile

In a QtW-BRW with sufficiently large number of unit-cells in Bragg reflectors, for the fundamental even mode, the field value at the interface of the core and the TBRs vanishes. In this sense, the Bragg mirrors resemble perfect conducting boundaries and the central portion of the field profile can be expressed as a cosine function with a half-period of t_c. Such a field profile, as can be seen in Fig. 3, consists of a central portion in the core and periodically interchanging out-of-phase and in-phase portions inside the TBRs. The absolute value of the ratio of the first out-of-phase lateral peak to the central peak can be obtained by simply using the continuity of tangential components of electric and magnetic fields at the interface between the core and the first layer of the periodic cladding as

$$\rho_c = \left(\frac{n_1}{n_c}\right)^{2f} \frac{k_c}{k_1}. \tag{9}$$

Due to the imaginary nature of the Bloch wavenumber in a BRW, the fields in the TBR decay swiftly in an oscillatory manner. The absolute value of the ratio of the adjacent peaks in the Bragg stack can be calculated from (6) as

$$\rho_{\mathrm{TBR}} = \left(\frac{n_1}{n_2}\right)^{2f} \frac{k_2}{k_1}. \tag{10}$$

In our analysis, each in/out-of phase part of the oscillating Bragg mode profile is replaced with a Gaussian approximation, $\psi_w(x)$, defined as

$$\psi_w(x) = \exp\left(-\frac{x^2}{w^2}\right). \tag{11}$$

with the according width, sign, and amplitude. It is well known that a cosine function with a half-period t is best fit to the Gaussian function, $\psi_w(x)$, when [16]

$$\frac{w}{t} = \frac{1}{\pi}. \tag{12}$$

As such, we approximate the field distribution of the core layer with a Gaussian function of width $w_c = t_c/\pi$. Similarly, the rest of the field distribution inside each unit-cell is approximated by a Gaussian function with $w = \Lambda/\pi$ as well. Using (9) and (10), and assuming the amplitude of each Gaussian function equal to the maximum value for each section, one can approximate the entire field profile as

$$\psi(x) = \psi_{t_c/\pi}(x) - \rho_c \sum_{m=0}^{N-1} (-\rho_{\mathrm{TBR}})^m \psi_{\Lambda/\pi}(x \pm \Delta_m) \tag{13}$$

where N is the number of unit-cells of Bragg reflectors and

$$\Delta_m = \frac{t_c + (2m+1)\Lambda}{2}. \tag{14}$$

Expression (13) offers an analytical form for the near-field approximation of the Bragg mode. We can now proceed to calculate the FF using the diffraction integral.

The contribution of the Gaussian function in (11) to the diffraction integral of (7) is given as

$$\Psi_w(\theta) = \cos(\theta)\xi_w(\theta), \tag{15}$$

$$\xi_w(\theta) = \frac{w}{\sqrt{2}} \exp[-[k_0 \sin(\theta) w]^2]. \tag{16}$$

Using (13) and (16), an approximate diffraction pattern for the waveguide is obtained as

$$I(\theta) \propto |\Psi(\theta)|^2 = \cos^2(\theta)[\xi_{t_c/\pi} + \rho_c \xi_{\Lambda/\pi} G(\theta)]^2 \tag{17}$$

where

$$G(\theta) = -2 \sum_{m=0}^{N-1} (-\rho_{\mathrm{TBR}})^m \cos[k_0 \sin(\theta) \Delta_m]. \tag{18}$$

In case of a semi-infinite structure or a BRW with an insignificant leakage loss, (18) can be further simplified as

$$G(\theta) \approx -2 \frac{\cos\left(k_0 \sin(\theta) \frac{t_c+\Lambda}{2}\right) + \rho_{\mathrm{TBR}} \cos\left(k_0 \sin(\theta) \frac{t_c-\Lambda}{2}\right)}{1 + \rho_{\mathrm{TBR}}^2 + 2\rho_{\mathrm{TBR}} \cos(k_0 \sin(\theta)\Lambda)}. \tag{19}$$

We examined the validity of the proposed model by applying it to the examples introduced in Table I. The resulting near and far fields are illustrated in Figs. 9 and 10 respectively. The approximate NF is calculated using (13) and is plotted together with the exact solution in Fig. 9. Similarly, in Fig. 10 the exact far fields are obtained using expression (7), whereas the approximation conveys the results of the model presented in (17). The two presented figures illustrate a good agreement between the exact and approximate NF and FF in all the examples, which in turn demonstrates the accuracy of the proposed model.

Thus far, the approximation was focused on the analysis of the FF of QtW-BRWs. As one moves away from the quarter-wave condition, (9) and (10) do not hold anymore therefore (4) should be employed. However, by inspecting the non-QtW examples presented in the previous section, illustrated in Fig. 11, it becomes evident that the presented approximation can also predict

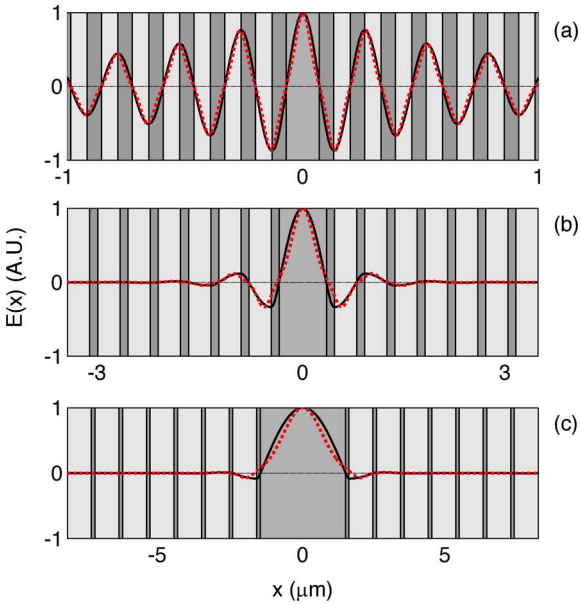

Fig. 9. Near field of the three design examples as given in Table I; exact (solid line) and approximate (dotted line).

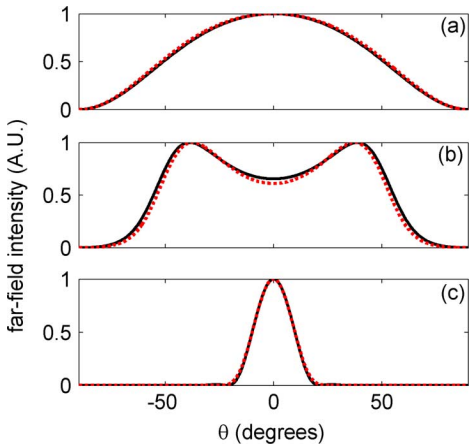

Fig. 10. Far field of the three design examples as given in Table I; exact (solid line) and approximate (dotted line).

the far field of such devices with good agreement. The only difficulty in applying the approximation to non-QtW BRWs is the complication in calculating the wavenumbers needed in (17).

It is also worth to note that a similar approach can be used to approximate the FF of any other field profile with analytically known NF characteristic and Gaussian-like lobes. Such modes may include higher order Bragg modes, asymmetric Bragg modes, and ARROW modes. However, the whole NF characteristics presented here should be changed accordingly for any of the above-mentioned analysis.

The benefits of a closed form approximation are well-known. In general, analytical approaches impart a useful intuition about the influence of the various waveguide parameters on the FF. In the approximation discussed here, detailed analysis of the FF behavior can be achieved by examining the equations derived here. Such analysis, which will be presented in the following section, can then be used to facilitate the design and optimization procedures.

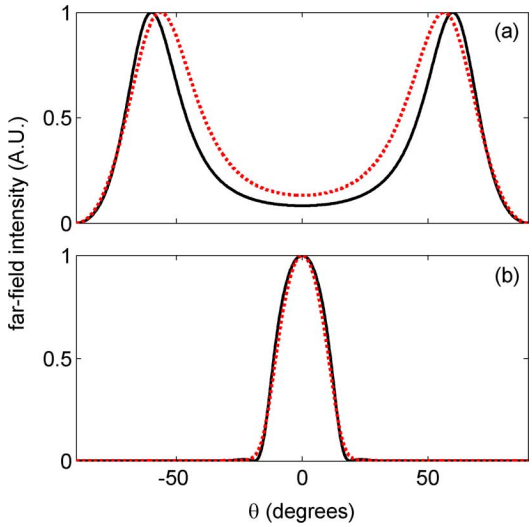

Fig. 11. Far-field distributions of the non-QtW Bragg waveguides defined in Table II; exact (solid line) and assuming quarter-wave (dotted line).

IV. Design Criteria

Manipulation and tailoring the far-field diffraction of an optical device is an essential design consideration for many photonic devices. In most practical applications, a single-lobed, low-divergence beam is desired for enhancing power coupling between optical elements. In Fig. 6 we showed that in some cases the FF of a Bragg mode can be a single lobe centered around $\theta = 0$. Here, we provide details of the conditions which lead to such characteristic.

In Section II we suggested that after a certain core thickness, the larger the core is, the more confined the FF will be. In order to evaluate this assumption, first we shall reformulate (17) as

$$\begin{aligned}\Psi(\theta) &= \xi_{t_c/\pi}\cos(\theta) + \rho_c \xi_{\Lambda/\pi} G(\theta)\cos(\theta) \\ &= \Psi_1(\theta) + \Psi_2(\theta). \end{aligned} \tag{20}$$

This expression is composed of two terms: the first term accounts for the FF of the field profile within the core layer, and the second term is associated with the far field resulting from the rest of the near field distribution. Examining these two terms separately elucidates the significant role which the first term plays in contributing to a single lobe in the FF.

The contribution of each of the two terms discussed above is illustrated in Fig. 12 for the design examples introduced in Table I. For design example D_1, the second term, Ψ_2, encounters one single extremum at $\theta = 0$. Therefore, although the two terms act to partially cancel each other out, the resulting FF is a single lobe. This takes place when the effective index is well below the stack refractive indices, which usually significantly increases the leakage losses of the waveguide when using finite Bragg stacks and is hence seldom used in practical structures. However, the behavior is different for D_2. As illustrated

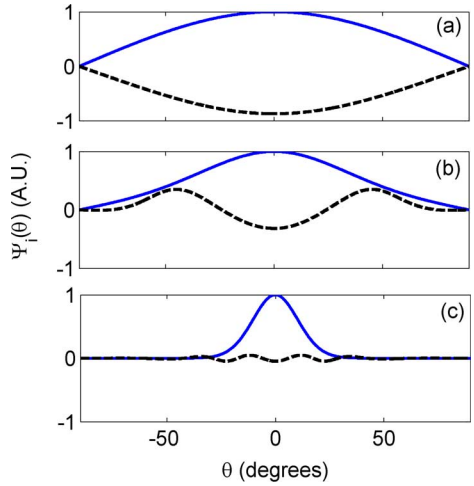

Fig. 12. Ψ_1 (solid line) and Ψ_2 (dashed line) expressed in (20) for the design examples studied in Table I. Both terms are normalized to the maximum of Ψ_1.

in Fig. 12, the second term has more than one extremum. Although the two lateral maxima have small values compared to the value at $\theta = 0$, the overall far-field pattern is double-lobed as a result of the destructive superposition of the two terms at the center. In the last example, D_3, Ψ_1 is much larger than Ψ_2 due to the large ratio of the peaks in (9), therefore leading to one single lobe in the superposition of the two terms.

The effect of Ψ_2 on the total far field can be quantitatively accounted for by examining the overall far field in the central region, $\Psi(0)$. From (20) and (19), this value can be expressed as

$$\Psi(0) \approx 1 - 2\frac{\rho_c}{1+\rho_{\mathrm{TBR}}} = 1 - 2\left(\frac{n_2}{n_c}\right)^{2f} \frac{k_c}{k_1 n_2^{2f} + k_2 n_1^{2f}}. \quad (21)$$

It can be clearly seen that Ψ_1 acts to partially cancel out Ψ_2 at the far-field center as discussed previously. Hence, disregarding the special cases in which Ψ_2 has only one extremum, it is deduced that the far-field profile will be closer to a single-lobed pattern for smaller second terms. As such, the condition of having a single lobe for the FF reduces to the examination of the wavenumbers and refractive indexes in different layers of BRWs, and can be expressed as

$$2\left(\frac{n_2}{n_c}\right)^{2f} \frac{k_c}{k_1 n_2^{2f} + k_2 n_1^{2f}} \ll 1. \quad (22)$$

A well confined single-lobed FF is essential for appropriate communication with other optical components. However single-lobed D_1-like structures are of no practical use due to the lossy nature of the Bragg mode. Hence, the only possibility to achieve a favorable FF profile is the structures which fulfill the above condition. In example D_3, on the contrary, where the mode is well confined in the core, the left-hand side of (22) reduces to 0.1441, which is sufficiently small to comply with the condition in (22). Such an equation is meant to provide a condition for single-lobed FF, and does not set any limitations on the spatial divergence. In order to improve the usefulness of this condition, an additional constraint can be introduced to limit the tolerable FF width for a given application. Due to our interest in well confined low-loss modes, it is possible to disregard the $\cos(\theta)$ term to further simplify the expression of the FF in (17). After some manipulation, the FWHM of the total FF can be approximated as

$$\mathrm{FWHM} \approx 2\sin^{-1}\left(\frac{\pi}{k_0 t_c}\sqrt{\frac{\ln 2}{2}}\right). \quad (23)$$

The constraints (22) and (23) provide a set of basic tools for designing BRWs with suitable, single-lobed and low divergence far-field profiles. However, not only the mentioned conditions can be used to achieve such FF properties, but also the Gaussian model presented in (17) itself can be adopted to further manipulate the far field in more complex settings.

V. Conclusion

The far-field behavior of the Bragg reflection waveguides has been studied in detail. It was demonstrated that through fine engineering of the structure, one can manipulate the far field of the fundamental Bragg mode to gain practical single-lobed far-field patterns. A Gaussian approximation was proposed for the fundamental Bragg mode of quarter-wave BRWs. By applying such an approximation, an analytical formula for calculation of the far-field diffraction pattern of a Bragg mode can be derived. The proposed model offers a simple and effective method for the far-field pattern calculations of BRWs and provides insight for device design and optimization.

References

[1] P. Yeh and A. Yariv, "Bragg Reflection waveguides," *Opt. Commun.*, vol. 19, no. 3, pp. 427–430, Dec. 1976.

[2] A. Yariv and P. Yeh, *Photonics: Optical Electronics in Modern Communications (The Oxford Series in Electrical and Computer Engineering)*. New York: Oxford Univ. Press.

[3] Y. Sakurai and F. Koyama, "Proposal of tunable hollow waveguide distributed Bragg reflectors," *Jpn. J. Appl. Phys.*, vol. 43, no. 5a, pp. L631–L633, Apr. 16, 2004.

[4] E. Simova and I. Golub, "Polarization splitter/combiner in high index contrast Bragg reflector waveguides," *Opt. Exp.*, vol. 11, pp. 3425–3430, 2003.

[5] N. Ponnampala m and R. G. DeCorby, "Self-assembled hollow waveguides with hybrid metal-dielectric Bragg claddings," *Opt. Exp.*, pp. 12595–12604, 2007.

[6] B. Bijlani, P. Abolghasem, and A. S. Helmy, "Second harmonic generation in ridge Bragg reflection waveguides," *Appl. Phys. Lett.*, vol. 92, no. 10, 2008, Art. ID 101124.

[7] P. Abolghasem and A. Helmy, "Matching layers in Bragg reflection waveguides for enhanced nonlinear interaction," *IEEE J. Quantum Electron.*, vol. 45, no. 6, pp. 646–653, Jun. 2009.

[8] A. S. Helmy, "Phase matching using Bragg reflection waveguides for monolithic nonlinear optics applications," *Opt. Exp.*, vol. 14, no. 3, pp. 1243–1252, Feb. 2006.

[9] R. Haidar, N. Forget, and E. Rosencher, "Optical parametric oscillation in microcavities based on isotropic semiconductors: A theoretical study," *IEEE J. Quantum Electron.*, vol. 39, no. 4, pp. 569–576, Apr. 2003 .

[10] A. Helmy, D. Hutchings, T. Kleckner, J. Marsh, A. Bryce, J. Arnold, C. Stanley, J. Aitchison, C. Brown, K. Moutzouris, and M. Ebrahimzadeh, "Quasi-phase-matching in GaAs-AlAs superlattice waveguides via bandgap tuning using quantum well intermixing," *Nonlin. Opt.: Mater., Fundam., Applicat.*, vol. 46, pp. 159–161, 2000.

[11] A. Fiore, S. Janz, L. Delobel, P. van der Meer, P. Bravetti, V. Berger, E. Rosencher, and J. Nagle, "Second-harmonic generation at lambda = 1.6 mu m in AlGaAs/Al203 waveguides using birefringence phase matching," *Appl. Phys. Lett.*, vol. 72, pp. 2942–2944, Jun. 8, 1998.

[12] J. B. Shellan, W. Ng, P. Yeh, A. Yariv , and A. Y. Cho, "Transverse Bragg-reflector injection lasers," *Opt. Lett.*, vol. 2, pp. 136–138, May 1978.
[13] J. Lee and S. Shin, "Strong discrimination of transverse modes in high-power laser diodes using Bragg channel waveguiding," *Opt. Lett.*, vol. 14, pp. 143–145, Jan. 1989.
[14] B. J. Bijlani and A. S. Helmy, "Bragg Reflection waveguide diode lasers," *Opt. Lett.*, vol. 34, pp. 3734–3736 , Dec. 1, 2009.
[15] M. Matsumoto, M. Taneya, S. Matsui, S. Yano, and T. Hijikata, "Single-lobed far-field pattern operation in a phased array with an integrated phase shifter," *Appl. Phys. Lett.*, vol. 50, no. 22, pp. 1541–1543, 1987.
[16] D. Botez, "Simple design rules for single-lobe operation of (evanescently coupled) index-guided phase-locked arrays of diode lasers," *IEEE J. Quantum Electron.*, vol. 24, no. 10, pp. 2034–2038, Oct. 1988.
[17] D. Scifres, W. Streifer, and R. Burnham, "Experimental and analytic studies of coupled multiple stripe diode lasers," *IEEE J. Quantum Electron.*, vol. QE-15, no. 9, pp. 917–922, Sep. 1979.
[18] M. Khajavikha n, A. Hoyer-Leitze l, and J. Leger, "Efficient conversion of light from sparse laser arrays into single-lobed far field using phase structures," *Opt. Lett.*, vol. 33, no. 20, pp. 2377–2379, Oct. 15, 2008.
[19] P. Ehbets, H. P. Herzig, R. Dändliker, P. Regnault, and I. Kjelberg, " Beam shaping of high-power laser diode arrays by continuous surface-relief elements," *J. Mod. Opt.*, vol. 40, pp. 637–645, Apr. 1993.
[20] B. R. West and A. S. Helmy, "Properties of the quarter-wave Bragg reflection waveguide: Theory," *J. Opt. Soc. Amer. B, Opt. Phys.*, vol. 23, no. 6, pp. 1207–1220, Jun. 2006.
[21] H. C. Casey and M. B. Panish, *Heterostructure Lasers Pt.A. Fundamental Principles*. New York: Academic, 1978.
[22] R. L. Lucke, "Rayleigh-Sommerfeld Fraunhofer diffraction," *ArXiv Phys. E-Prints*, Apr. 2006.
[23] S. Gehrsitz, F. K. Reinhart, C. Gourgon, N. Herres, A. Vonlanthen, and H. Sigg, "The refractive index of $Al_xGa_{1x}As$ below the band gap: Accurate determination and empirical modeling," *J. Appl. Phys.*, vol. 87, no. 11, pp. 7825–7837, 2000.

Nima Zareian was born in Tehran, Iran, in 1983. He received the B.Sc. degree from Isfahan University of Technology, Isfahan, Iran, in 2001 and the M.Sc. degree from Sharif University of Technology, Tehran, Iran, in 2007, both in electrical engineering. He is currently working towards the Ph.D. degree in University of Toronto, Toronto, ON, Canada.

His current research interests include periodic structures, integrated nonlinear optical devices, and III-V semiconductor diode lasers.

Mr. Zareian is a student member of SPIE.

Payam Abolghasem (M'10) received the B.A.Sc. degree in electrical engineering from the University of Ottawa, Ottawa, ON, Canada, in 2004, and the M.A.Sc. from McMaster University, Hamilton, ON, Canada, in 2006. He is currently working toward the Ph.D. degree at the University of Toronto, Toronto, ON, Canada.

His research interests are in nonlinear optical properties in III-V semiconductor materials, integrated optical parametric devices, semiconductor diode lasers, and computational electromagnetics.

Amr S. Helmy (M'99–SM'06) received the B.Sc. degree in electronics and telecommunications engineering from Cairo University, Cairo, Egypt, in 1993, and the M.Sc. and Ph.D. degrees with a focus on photonic fabrication technologies from the University of Glasgow, Glasgow, U.K., in 1994 and 1999, respectively.

Prior to his academic career, he was with Agilent Technologies Photonic Devices, R&D Division, in the U.K. At Agilent, his responsibilities included developing distributed feedback lasers, monolithically integrated lasers, modulators, and amplifiers in InP-based semiconductors. He also developed high-powered submarine-class 980-nm InGaAs pump lasers. He is currently an Associate Professor with the Edward S. Rogers Sr. Department of Electrical and Computer Engineering, University of Toronto, Toronto, ON, Canada. His research interests include photonic device physics and characterization techniques, with emphasis on nonlinear optics in III-V semiconductors; applied optical spectroscopy in III-V optoelectronic devices and materials; and III-V fabrication and monolithic integration techniques.

Dr. Helmy is a member of the Optical Society of America.